Electronic Supplementary Material (ESI) for Dalton Transactions.

Supplementary materials

Crumpled graphene microspheres anchored with $NiCo_2O_4$ nanoparticles as advanced composite electrode for asymmetric supercapacitor with ultralong cycling life

Ruiwen Yuan, Wenxiao Chen, Jingyuan Zhang, Lu Zhang, Hao Ren, Tianyu Miao, Zhuo Wang, Ke Zhan, Min Zhu, Bin Zhao*

School of Materials and Chemistry, University of Shanghai for Science and Technology, Shanghai 200093, China

*Corresponding Author: Bin Zhao

E-mail: zhaobin@usst.edu.cn

Table S1. Elemental composition from EDS analysis for the composites annealed at different temperatures.

Annealing temperature	**C (at. %)**	**O (at. %)**	**Ni (at. %)**	**Co (at. %)**
300 ℃	57.84	16.50	10.57	15.08
350 ℃	31.47	21.89	18.24	28.40
400 ℃	21.04	19.77	22.67	36.52

Table S2. Surface area and pore volume of $NiCo_2O_4$/CGM composites fabricated with different GO/precursor ratios.

Samples	**Specific surface area ($m^2\ g^{-1}$)**	**Pore volume ($cm^3\ g^{-1}$)**
NC-0.5	141.65	0.36
NC-1	150.98	0.53
NC-1.5	61.66	0.31
NC-2	49.86	0.34

Table S3. Comparison of electrochemical performance with previous studies

Electrode materials	**Synthesis method**	**Capacitance ($F\ g^{-1}$) ($1\ A\ g^{-1}$)**	**Cycling stability Cycles/%**	**Ref.**
$NiCo_2O_4$/CGM	spray-assisted self-assembly	369.5	15000/98%	This work
MnO@C/graphene	Spray pyrolysis	264	6000/80%	[1]
Fe_3O_4/rGO	Spray pyrolysis	269	2000/80%	[2]
ZIF-8/rGO	Supersonic spray	336	10000/96%	[3]
$MnFe_2O_4$/CG	Spray pyrolysis	195	5000/31%	[4]
$K_2Ti_6O_{13}$/rGO	Spray pyrolysis	275	2000/83%	[5]
MnO_2 /CNT	Spray pyrolysis	340	4000/100%	[6]
$CoFe_2O_4$/graphene	Spray pyrolysis	302	2000/86%	[7]
FeO_x/MWCNT	Spray suspension	312 ($2\ mV\ s^{-1}$)	150/80%	[8]
MnO_2/C	aerosol-assisted spray	412 ($2\ mV\ s^{-1}$)	4300/88%	[9]

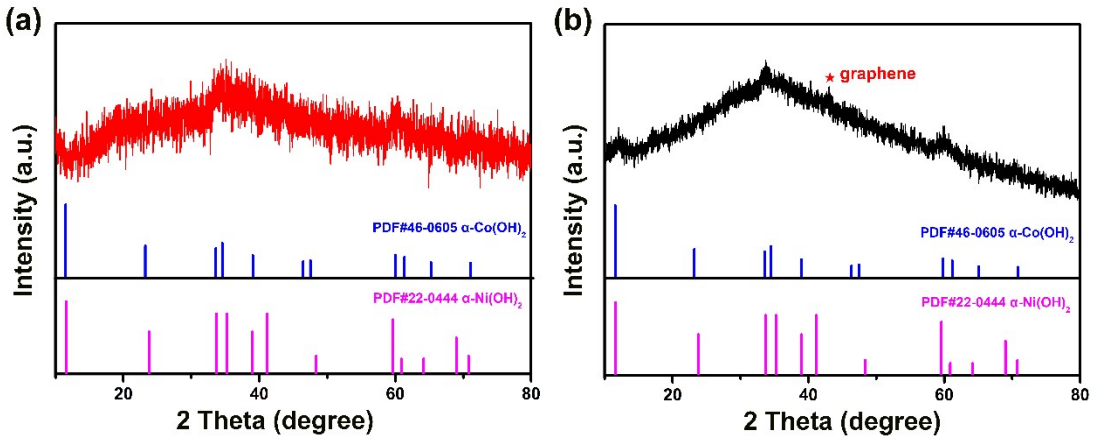

Fig. S1. XRD patterns of (a) nickel-cobalt hydroxide precursor and (b) hydroxide/CGM intermediate before annealing.

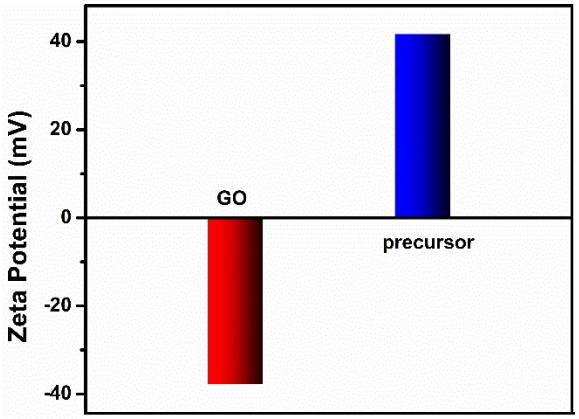

Fig. S2. Zeta potential measurements of GO (a) and precursor (b).

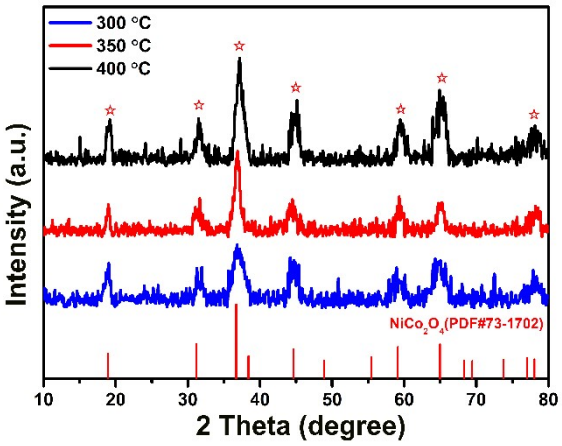

Fig. S3. XRD patterns of the $NiCo_2O_4$/CGM composites (GO/hydroxide ratio of 1:1) annealed at different temperatures.

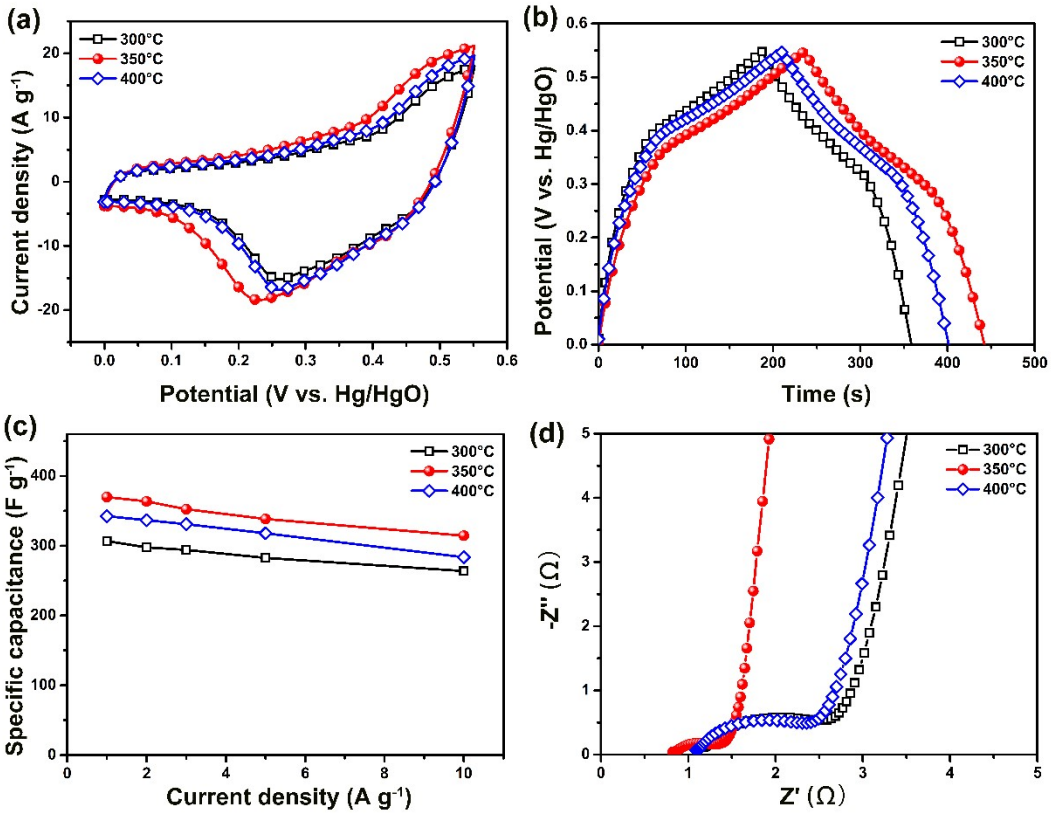

Fig. S4. Electrochemical performance of the $NiCo_2O_4$/CGM (GO/hydroxide ratio of 1:1) annealed at different temperatures: (a) CV curves at 30 mV s^{-1}; (b) GCDs at various current densities; (c) Specific capacitance as a function of current density; (d) Nyquist plots.

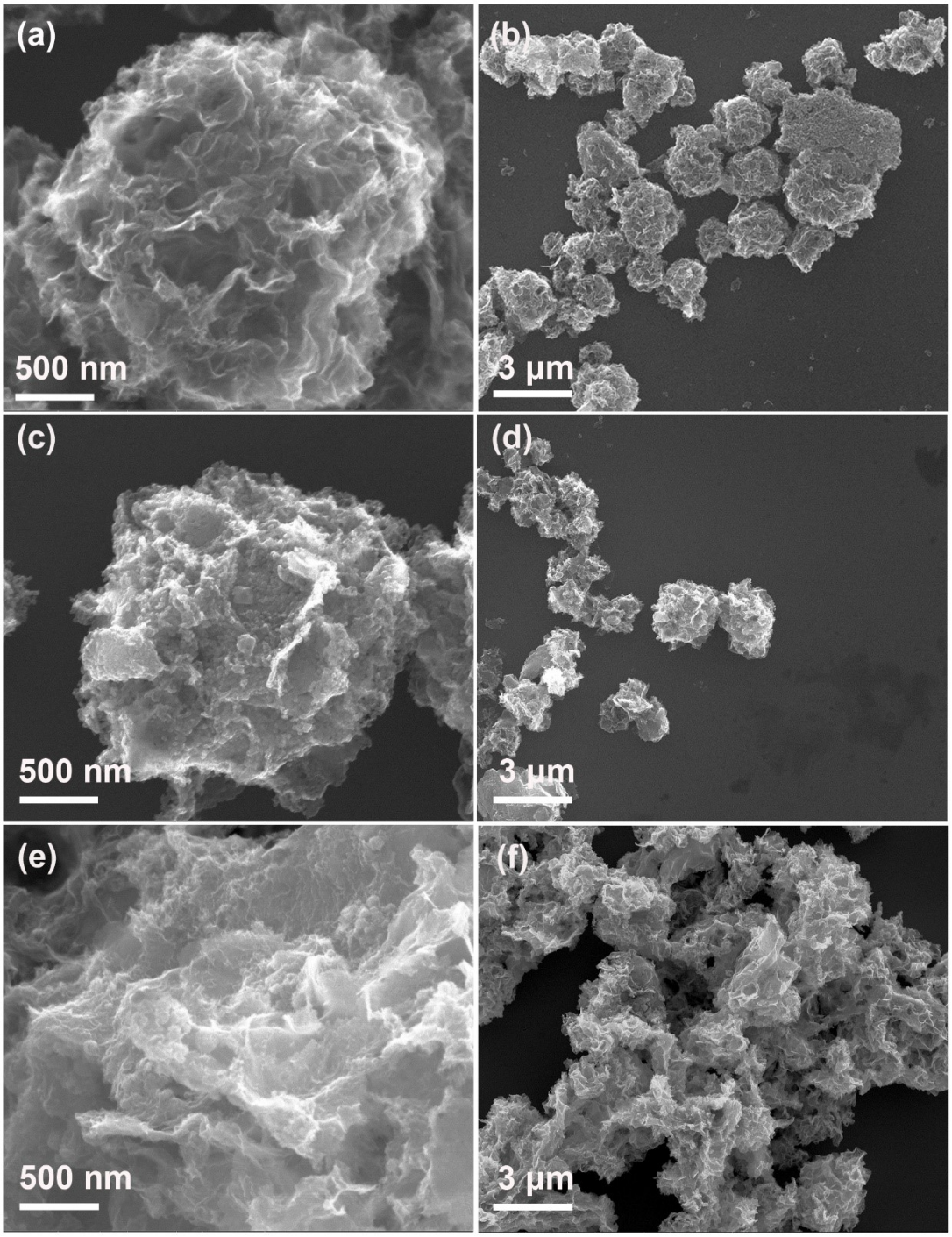

Fig. S5. SEM images of (a-b) NC-0.5; (c-d) NC-1.5; (e-f) NC-2.

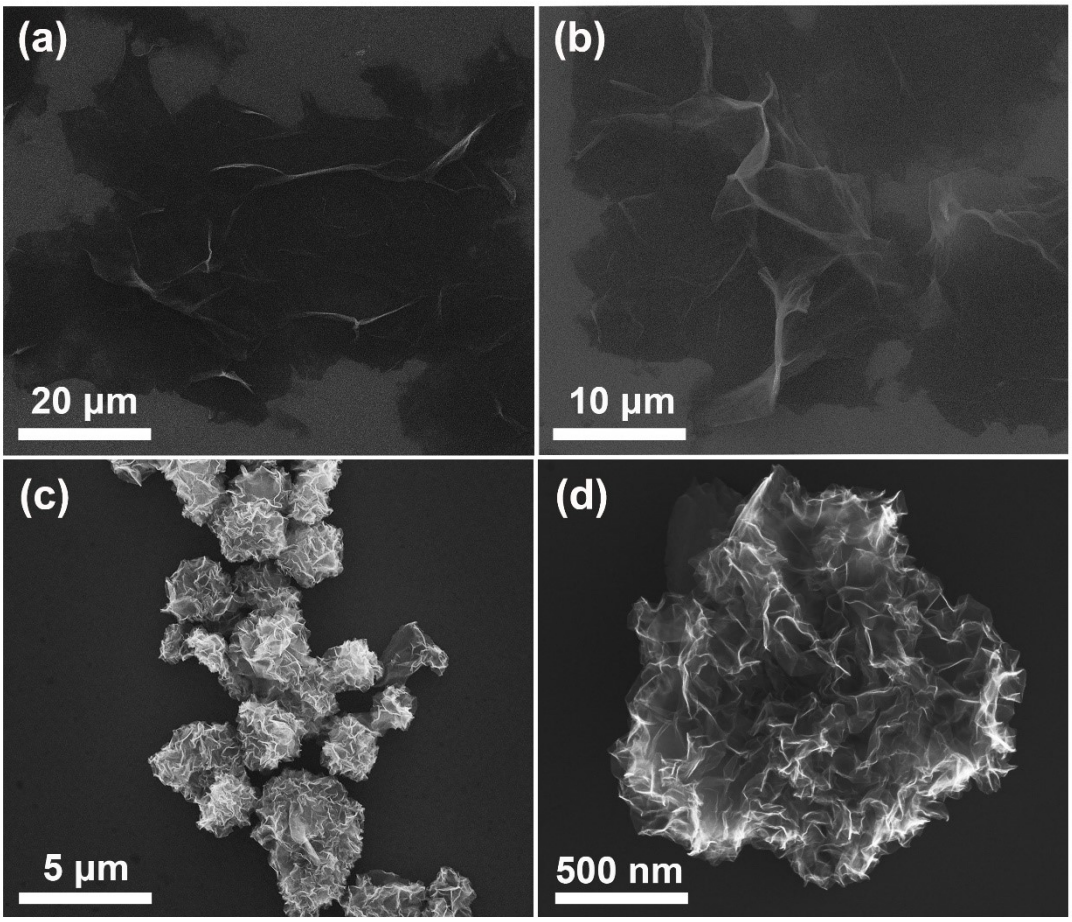

Fig. S6. SEM images of GO (a-b) and pure CGM (c-d).

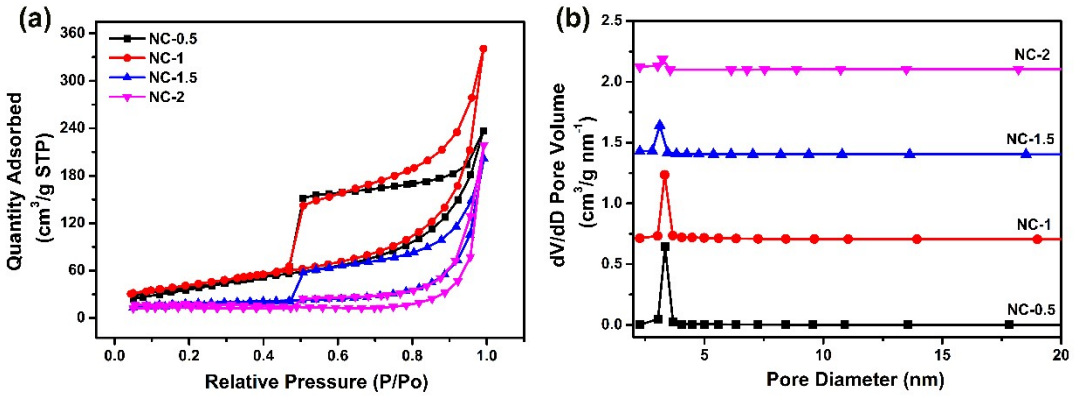

Fig. S7. Nitrogen adsorption/desorption isotherms (a) and BJH pore size distribution (b) of $NiCo_2O_4$/CGM composites fabricated with different GO/precursor ratios.

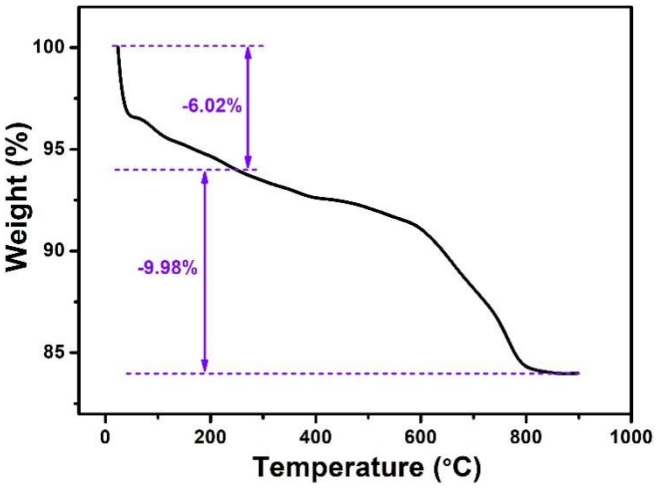

Fig. S8. Thermogravimetric analysis (TGA) curves of the NC-1 composite.

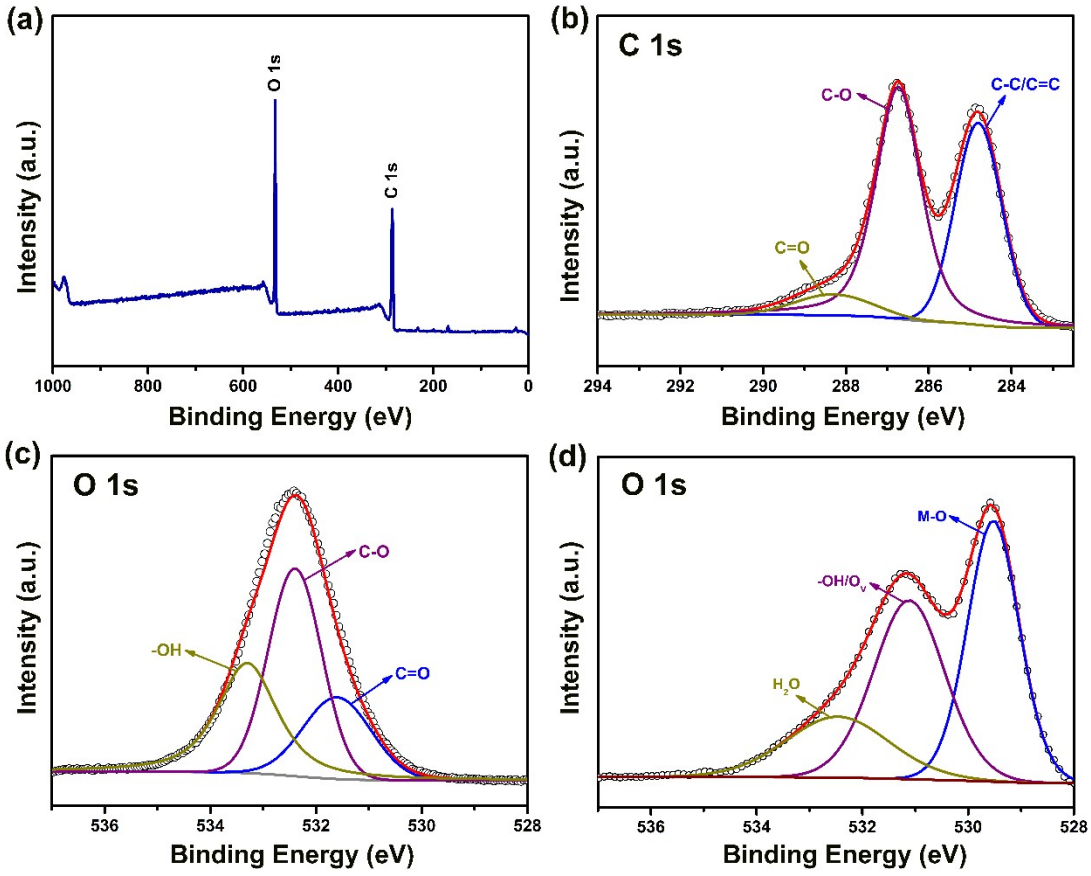

Fig. S9. XPS spectra of GO: (a) survey spectrum; high-resolution spectrum of C 1s (b) and O 1s (c); (d) high-resolution O 1s spectrum of the NC-1 composite.

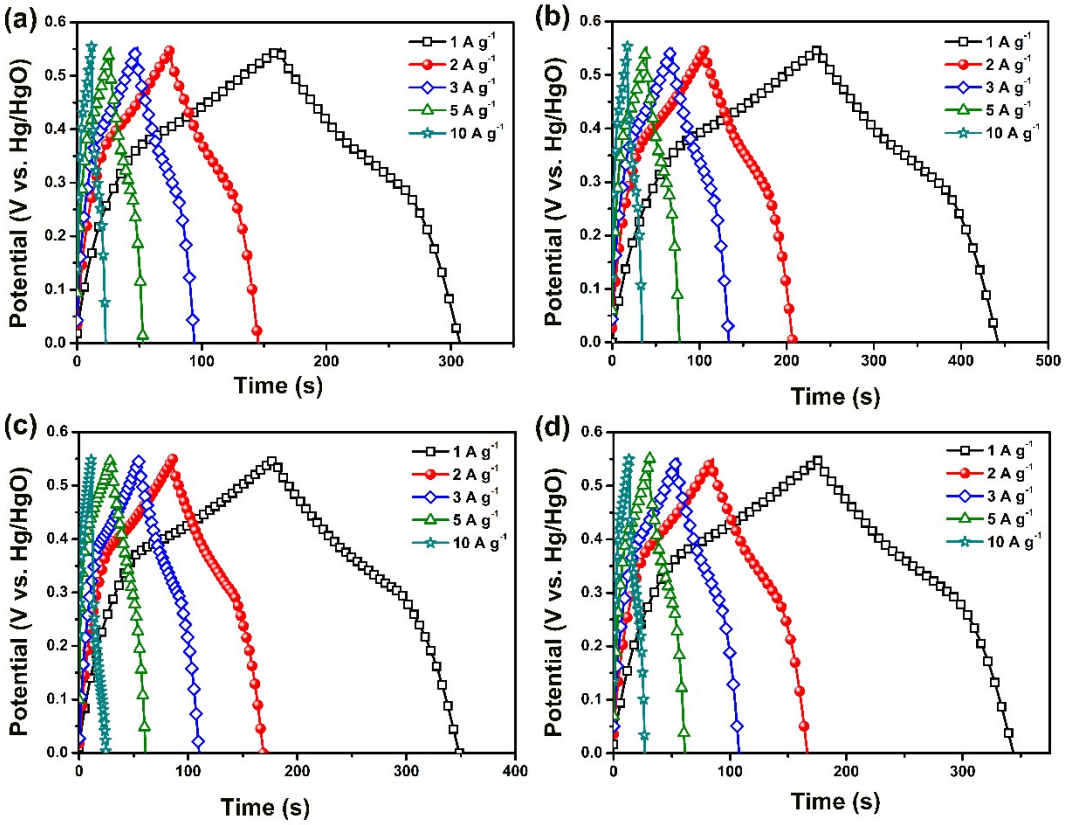

Fig. S10. GCD curves at various scan rates for the NC-X composites: (a) NC-0.5; (b) NC-1; (c) NC-1.5 and (d) NC-2.

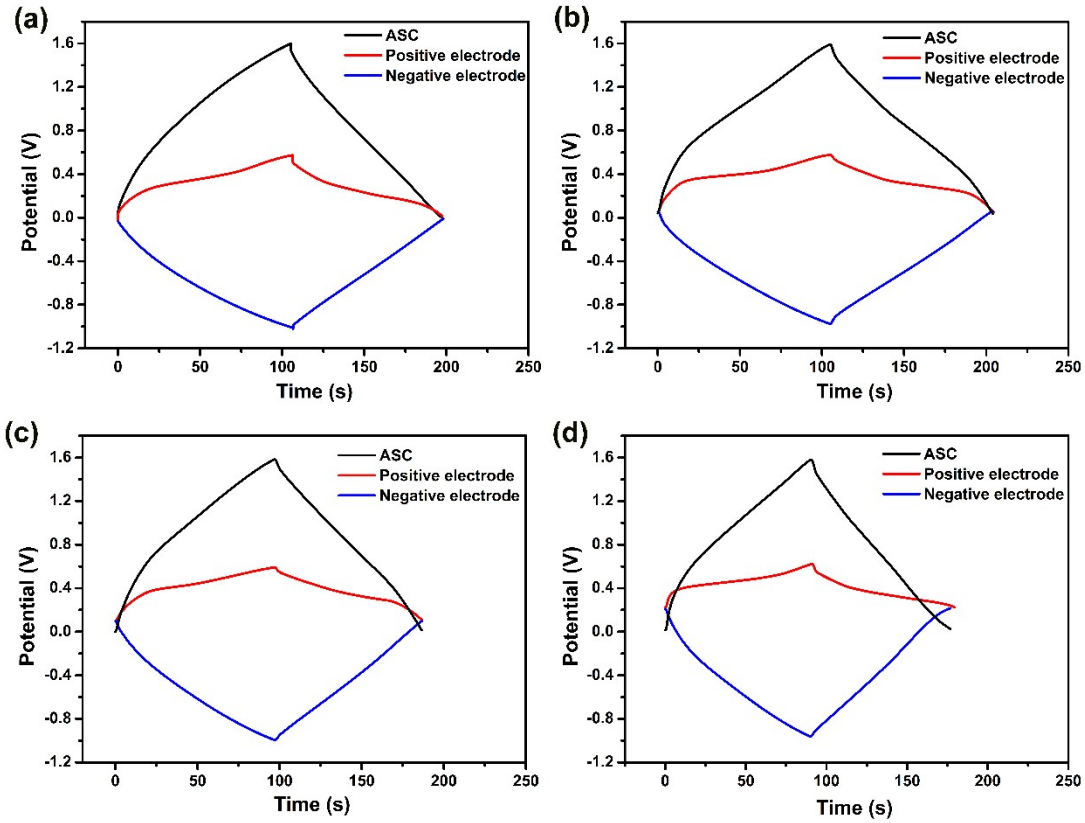

Fig. S11. GCD curves at 1 A g^{-1} for the positive and negative electrodes with the mass ratio of the positive and negative electrodes at (a) 1:1.5; (b) 1:2; (c) 1:2.5 and (d) 1:3.

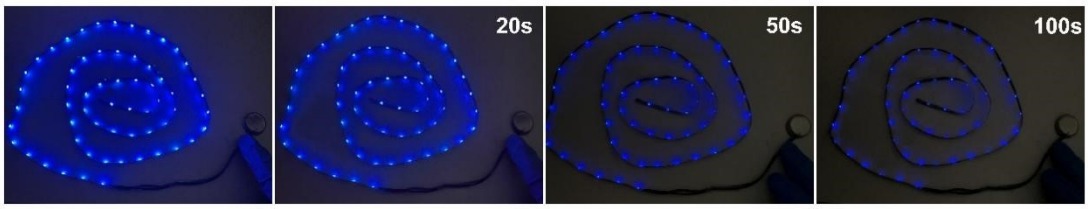

Fig. S12. LED strip powered by two ASC devices connected in series.

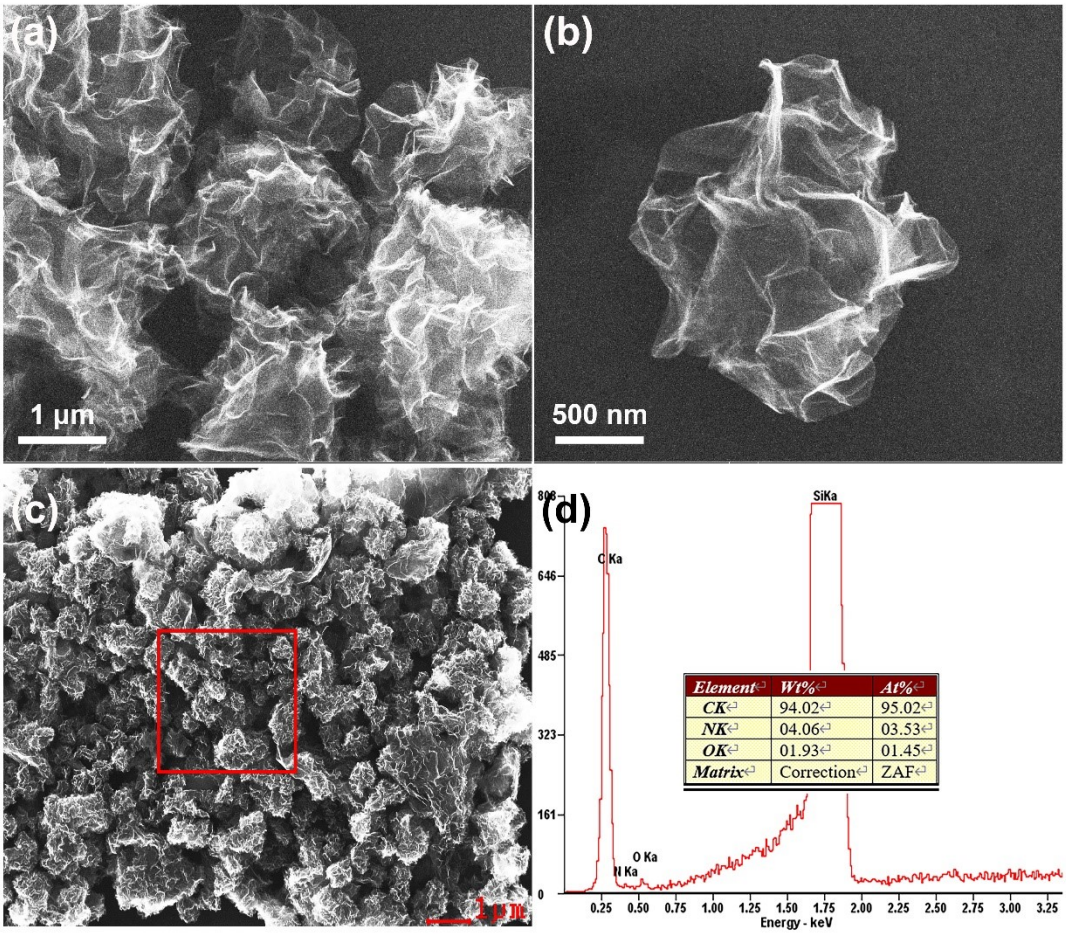

Fig. S13. SEM images and EDS spectrum of the N-CGM fabricated with GO/urea ratio of 1:30 at 800 ℃.

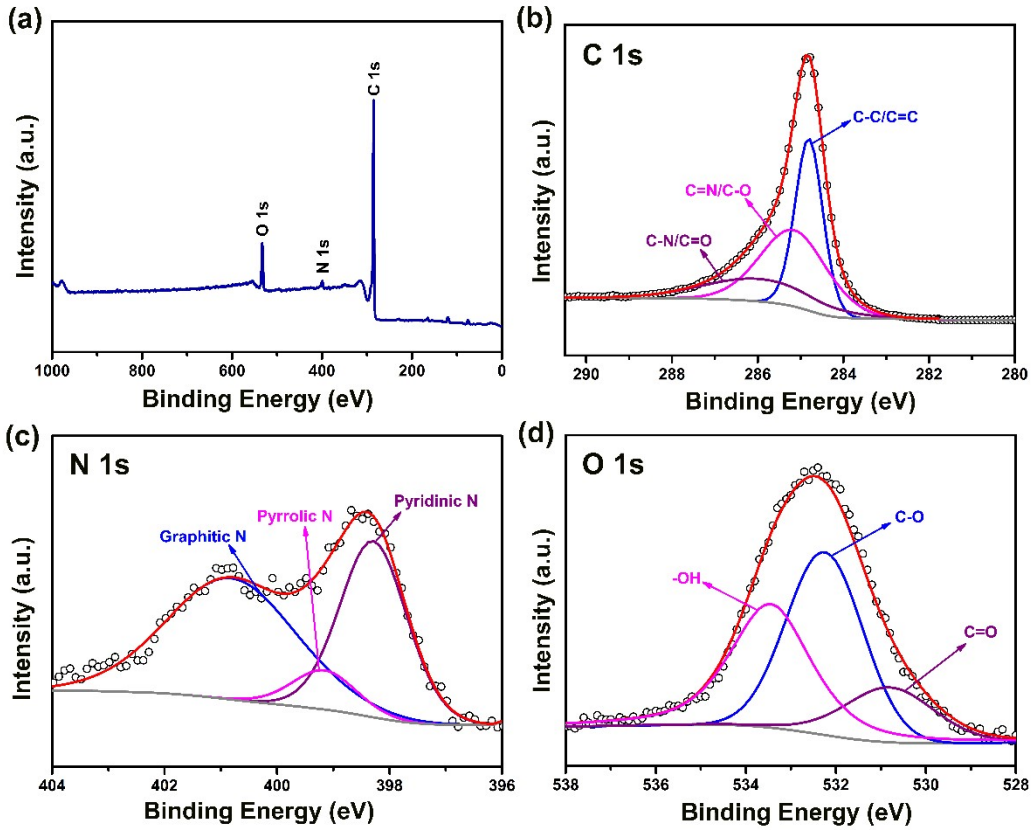

Fig. S14. XPS spectra of the N-CGM fabricated with GO/urea ratio of 1:30 at 800 ℃.

(a) survey spectrum; high- resolution spectrum of C1s (b), N 1s (c) and O 1s (d).

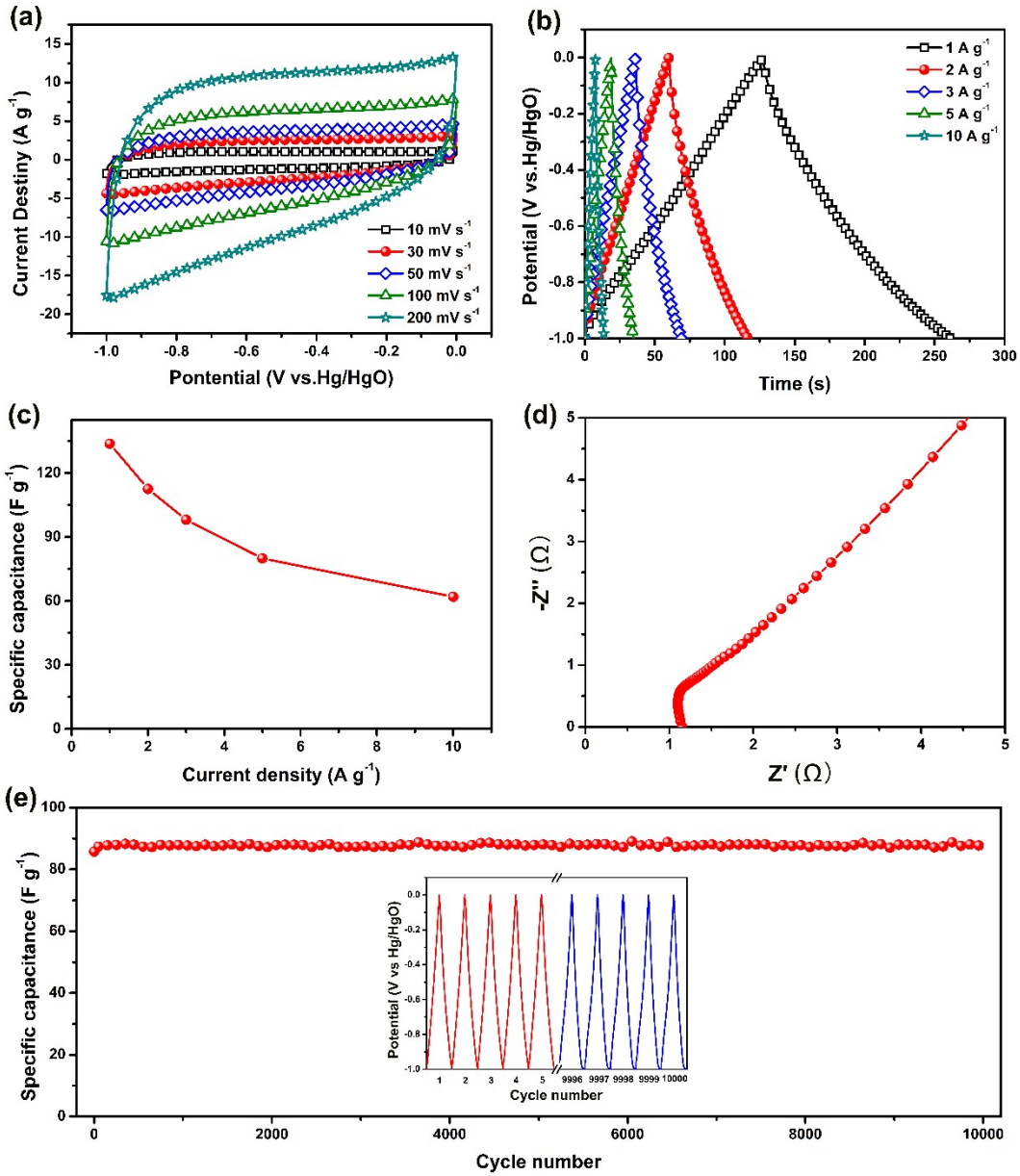

Fig. S15. Electrochemical performance of the N-CGM: (a) CV curves at various scan rates; (b) GCDs at various current densities; (c) Specific capacitance as a function of current density; (d) Nyquist plots; (e) Cycling stability at 5 A g^{-1} (The inset shows the GCD curves for the initial five cycles and the last five cycles).

The surface morphology of the N-CGM was observed by SEM, Fig. S13(a-b) show the microscopic morphology of N-CGM, which presents the typical crumpled microsphere. The overall shape of the microspheres is similar to that of sea urchins, and the diameter of the microspheres ranges from 2 to 3 μm. The N content in the N-CGM composite is about 3.53 at.% via EDS analysis.

To investigate the elemental composition state of N-CGM, X-ray photoelectron spectroscopy (XPS) was performed on N-CGM. Fig. S14(a) shows the measured spectrum of N-CGM without the remaining impurity elements except for C, N and O. The high-resolution C 1s spectrum (Fig. S14(b)) can be deconvoluted into three peaks located at 284.8, 285.3 and 286.2 eV. The peak at 284.8 eV corresponds to C-C/C=C, while the two peaks at 285.3 and 286.2 eV correspond to the two bonding structures of N-C bonds: N=C and N-C[10]. For the N 1s spectra in Fig. S14(c), the peaks at 398.3 and 399.2 eV correspond to "pyridine" and "pyrrole" N, respectively, which are N atoms in a π conjugated system, contributing to a π system with one or two p-electrons, respectively. The peak at 400.9 eV corresponds to "graphitic" N, which refers to the substitution of N atoms for C atoms inside the graphene layer[11-13]. The O 1s (Fig. S14(d)) at 531.8 eV can be regarded as the oxygen or water absorbed on the surface of sample[12].

The electrochemical performance of N-CGM in 1 M KOH electrolyte was evaluated by cyclic voltammetry (CV) and galvanostatic charge-discharge (GCD) measurements. Fig. S15(a) shows the typical CV curves of various N-CGM composites at different scan rates. The CV curves at all scan rates have a quasi-rectangular shape, showing their electrical double-layer behavior, and even at a scan rate of 200 mV s^{-1}, the curves are close to rectangular, indicating their superior rate capability. Fig. S15(b) shows the

GCD curves at different current densities. The GCD curves for N-CGM materials exhibit excellent symmetry and reveal a good reversibility. The specific capacitance can be calculated for different current densities based on the discharge time, the corresponding specific capacitances are 133.8, 112.6, 98.1, 80 and 62 F g^{-1} for current densities of 1, 2, 3, 5 and 10 A g^{-1} respectively. As the current density increases from 1 to 10 A g^{-1}, approximately 46.8% of the initial capacitance is retained. Fig. S15(c) illustrates the specific capacitance of N-CGM composites as a function of current density. The Nyquist plot of electrodes (Fig. S15(d)) has a small equivalent series resistance (ESR) in the high frequency region, and the almost invisible distinct semicircular arcs indicate that all electrodes have a small charge transfer resistance (Rct). In the low frequency region, the slope of the Nyquist plot represents the Warburg impedance, which is related to the ion diffusion in the electrode material. Fig. S15(e) shows the cycling stability of N-CGM at a current density of 5A g^{-1}. After 10,000 cycles, 100% of the initial specific capacitance is maintained, demonstrating excellent cycling stability.

References

1. X. Yang, X. Liu, Y. Wang, X. Liu, Z. Kong, A. Fu, Y. Li, P. Guo, H. Li and G. Song, *Energy Technol.*, 2019, **7**, 1800625.
2. C. Lee, E. H. Jo, S. K. Kim, J.-H. Choi, H. Chang and H. D. Jang, *Carbon*, 2017, **115**, 331-337.
3. E. Samuel, B. Joshi, C. Park, A. Aldalbahi, M. Rahaman and S. S. Yoon, *Electrochimica Acta*, 2020, **362**.
4. L. H. Nonaka, T. S. D. Almeida, C. B. Aquino, S. H. Domingues, R. V. Salvatierra and V. H. R. Souza, *ACS Appl. Nano Mater.*, 2020, **3**, 4859-4869.
5. C. Lee, S. K. Kim, H. Chang and H. D. Jang, *Nanomicro Lett*, 2019, **12**, 10.
6. D. Gueon and J. H. Moon, *ACS Sustainable Chemistry & Engineering*, 2017, **5**, 2445-2453.
7. C. Lee, S. K. Kim, J.-H. Choi, H. Chang and H. D. Jang, *Journal of Alloys and Compounds*, 2018, **735**, 2030-2037.
8. L. O'Neill, C. Johnston and P. S. Grant, *Journal of Power Sources*, 2015, **274**, 907-

915.

9. X. Wang, X. Fan, G. Li, M. Li, X. Xiao, A. Yu and Z. Chen, *Carbon*, 2015, **93**, 258-265.

10. C. Sathiskumar, S. Ramakrishnan, M. Vinothkannan, S. Karthikeyan, D. J. Yoo and A. Rhan Kim, *Nanomaterials* 2019, **10**.

11. H. Wang, C. Zhang, Z. Liu, L. Wang, P. Han, H. Xu, K. Zhang, S. Dong, J. Yao and G. Cui, *J. Mater. Chem.*, 2011, **21**.

12. L. Y. Wei DC, Wang Y, Zhang HL, Huang LP, Yu G., *Nano Lett*, 2009, **9**（**5**）, 1572-1578.

13. Y. Zhang, P. Li, X. Yin, Y. Yan, K. Zhan, J. Yang and B. Zhao, *RSC Adv.*, 2017, **7**, 50246-50253.